

# Feature Analysis of Functional MRI for Discrimination Between Normal and Epileptogenic Brain

Lauren S. Burrell, Simon M. Glynn, George J. Vachtsevanos, and Brian Litt

**Abstract**—Temporal lobe epilepsy (TLE) is the most common epilepsy syndrome in adults. As it is a focal disorder, i.e. limited to a particular area of the brain, it is often curable through surgery when drug therapies fail to control seizures. In order to ensure successful surgical outcome, the abnormal brain regions must be localized as accurately as possible to prevent the removal of healthy tissue. We report on a novel voxel-based procedure for discrimination between normal and epileptogenic brain tissue through feature analysis of continuous arterial spin labeling (ASL) perfusion functional magnetic resonance imaging (fMRI) data. Five TLE patients and three healthy controls were studied. Features were extracted from the fMRI time series of each subject to determine which individual features and combinations of features could correctly separate epileptogenic and normal brain tissue.

**Keywords** — Feature extraction; genetic programming; functional magnetic resonance imaging (fMRI).

## I. INTRODUCTION

EPILEPSY, a chronic neurological disorder characterized by recurrent, unprovoked seizures, affects approximately 60 million people worldwide [1]. For one-third of epilepsy patients, seizure control cannot be achieved through antiepileptic drug therapy; however, 7%–8% are candidates for surgical treatment. Successful outcome following resective surgery depends on accurate localization of the seizure onset zone. Currently, electroencephalography (EEG) is the most widely used tool for diagnosis and classification of epileptic disorders; however, the relatively low spatial resolution of EEG makes precise localization of epileptic activity difficult. In the absence of structural abnormalities, such as lesions or tumors, which might pinpoint the area of seizure onset, other functional methods are needed to localize the epileptogenic zone.

Functional magnetic resonance imaging (fMRI) is a non-invasive neuroimaging technique with higher spatial resolution than EEG that has the potential to localize epileptic activity. Functional MRI indirectly measures neural activity through detection of changes in blood flow, blood volume, and oxygen consumption. As regional brain function increases, there is a corresponding increase in regional cerebral blood flow (CBF). Blood oxygen level dependent (BOLD) fMRI exploits changes in concentrations of oxy- and deoxyhemoglobin that accompany changes in neural activity. The

differences in the magnetic properties of these substances provide the contrast in BOLD images. Arterial spin labeling (ASL) perfusion fMRI contrast is also a reflection of blood flow changes. During ASL perfusion scans, arterial blood water near the area of interest is electromagnetically labeled by a radiofrequency pulse to allow tracking of the CBF. Immediately after imaging of the pre-labeled spins, control images without labeled spins are acquired. Through pairwise subtraction of these label and control pairs, the effects of labeling can be determined, and CBF can be calculated.

BOLD fMRI generally has higher SNR and temporal resolution and larger signal changes due to activation than ASL perfusion [2]. BOLD contrast is also easier to measure, so it is the more widely used technique. Despite these technical challenges, ASL perfusion contrast has important characteristics that make it useful. First, the ASL imaging approach provides a physiological measure of CBF, while the BOLD technique only provides information about relative changes in the blood oxygen. Second, ASL also has the ability to measure resting function, which cannot be easily observed with BOLD contrast. Finally, ASL perfusion fMRI does not suffer from low frequency drift; therefore, long epochs of data can be examined for slowly evolving changes, which cannot be reliably detected by BOLD fMRI.

To date, ASL perfusion fMRI primarily has been used to examine the mean cerebral blood flow. Wolf et al. detected mesial temporal lobe hypoperfusion – decreased blood flow – in temporal lobe epilepsy patients using continuous ASL perfusion data [3]. In this study, we characterize the entire ASL perfusion signal through analysis of features of the CBF time series, as well as the mean CBF difference between normal and epileptogenic brain regions to identify additional features to lateralize temporal lobe epilepsy. Evaluating these features of perfusion data, in addition to the traditional mean CBF measure, could potentially provide physicians better tools for localizing seizure activity and allow them to concentrate solely on the dysfunctional areas when intervening surgically. This in turn reduces the risks of surgical complications, such as loss of memory or language function.

## II. METHODOLOGY

### A. Data

Resting ASL perfusion fMRI scans of five temporal lobe epilepsy patients and three healthy controls were obtained from the Center for Functional Neuroimaging at the University of Pennsylvania. All subjects provided informed consent in accordance with Institutional Review Board guidelines. The three healthy subjects hereafter referred to as Con1,

This work was supported by the National Institutes of health grants NIH R01-NS048598-01 / R01-NS041811-01 / K12-RR017625, the Klingenstein Foundation, the Whitaker Foundation, the Dana Foundation and The Epilepsy Therapy Development Project.

L. S. Burrell and G. J. Vachtsevanos are with the Georgia Institute of Technology, Atlanta, GA 30332 USA.

S. M. Glynn and B. Litt are with the Hospital of the University of Pennsylvania, Philadelphia, PA 19104 USA.

Con2, and Con3 were analyzed to serve as controls for this experiment. All subjects were made comfortable using head padding and told to sleep. Increased interictal (between seizure) epileptiform activity on EEG often accompanies sleep in patients with temporal lobe epilepsy [4], so we hypothesized that allowing the subjects to sleep would increase the likelihood of epileptic activity during the scan. After scanning, all subjects reported falling asleep during the scan; however, no information was available about when they fell asleep or the stage of sleep.

The resting perfusion images were collected during consecutive ten-minute scanning sessions at 3T with a repetition time of three seconds. All subjects, except for one control (Con1) and one patient (Pt5), were scanned for forty minutes. Con1 was scanned for twenty minutes, and Pt5 was scanned for thirty minutes. Each ten-minute functional dataset contains a total of 200 images. The raw ASL images consist of 16 slices (two-dimensional cross-sectional images of the brain) that are  $64 \times 64$  voxels. The voxel resolution is  $3.44 \times 3.44 \times 7.50 \text{ mm}^3$ . The odd numbered scans are label images, and the even numbered scans are control images.

Masks of the hippocampi of all subjects were manually segmented by a neurologist (S.M.G.). All of the subsequent analysis was limited to this region of interest (ROI). As the hippocampus, which is part of the mesial temporal lobe, is often a major contributor to the epileptic activity in patients with temporal lobe epilepsy, it is logical to focus in on this area.

Prior to the functional scanning, each of the five patients had EEG recordings taken that showed interictal spikes in one temporal lobe. During extended video EEG monitoring, all but one, Pt4, had seizures clearly originating in a single temporal lobe. One left temporal and two right temporal seizures were recorded for this patient. Anatomical MRI scans showed right mesial temporal sclerosis – a lesion commonly found in adults with TLE – in Pt2 and bilateral hippocampal volume loss in Pt5, with the right hippocampus being smaller than the left. The other three patients had normal brain structure. Four of the five patients also had positron emission tomography (PET) scans taken to look for evidence of hypometabolism in the temporal lobe, which is common in TLE patients. Pt4 had a normal PET scan. Pt1 and Pt5 showed hypometabolism in the temporal lobe in which the seizures were recorded, and Pt2 exhibited hypometabolism in the epileptogenic hemisphere but not the temporal lobe itself. Physicians combined this clinical information to determine the seizure onset side for each patient. For Pt4, it was not completely clear whether the disease was bilateral or unilateral, but the presumed epileptogenic zone was chosen.

### B. Preprocessing

Before the images were analyzed, they were preprocessed to reduce artifacts and noise corruption. The images were realigned slice-by-slice to the first functional image in order to account for signal changes due to subject motion during scanning and to reduce artifacts in the final CBF images [5]. An 8 mm full width at half maximum Gaussian smoothing

kernel was then applied to increase the overall signal-to-noise ratio (SNR), while also limiting the low-frequency noise amplification caused by spatial smoothing with too large a kernel [6]. Following realignment, the functional and anatomical images were co-registered so that they lined up evenly with one another. Through pairwise subtraction of adjacent label and control images, the perfusion images were calculated from the preprocessed ASL scans. This operation resulted in a total of 100 perfusion images for each ten-minute functional run. The CBF images, which are simply scaled versions of the perfusion images, were then computed. The voxel intensities in these images represent blood flow in physiological units of mL/100g/min. As every brain has unique shape, size, and structure, all CBF images were subsequently normalized to a  $3 \times 3 \times 3 \text{ mm}^3$  Montreal Neurological Institute (MNI) template for comparison across patients. Normalization warps images so that they conform to the space of a standard template brain [7]. The resulting dimensions of the normalized images were  $53 \times 63 \times 46$  voxels. All realignment, co-registration, normalization, and smoothing were performed with Statistical Parametric Mapping software (SPM2) [5, 7, 8].

### C. Feature Extraction

The voxel time course is a signal corresponding to the change in a voxel's intensity throughout time. Each image is a three-dimensional array representing the signal intensities of the voxels at a single point in time. By extracting the voxel intensity from the images at every time point, the voxel time course can be obtained as shown in Figure 1. Before these time signals were analyzed, they were rescaled to the range  $[-1, 1]$  to ensure that intrinsic differences in the mean CBF values of the left and right mesial temporal lobes did not affect the feature separability of the two classes. The time series from the individual ten-minute functional scans were concatenated to study the temporal dynamics of CBF over long periods of time.

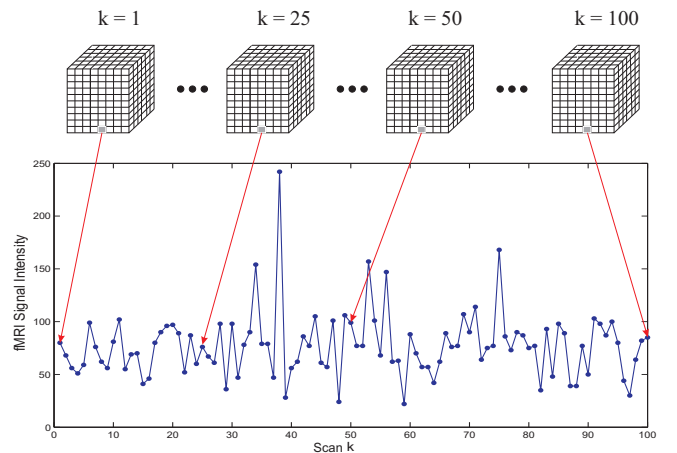


Fig. 1. fMRI time course extraction.

The features listed in Table I were extracted from the time courses of the mesial temporal voxels to determine which, if

TABLE I  
CLASSICAL FEATURE SET FOR fMRI ANALYSIS

Feature	Formula
Energy	$\sum_i x_i^2$
Curve Length	$\sum_i  x_i - x_{i-1} $
Nonlinear (Teager) Energy	$\sum_i (x_i^2 - x_{i+1} \cdot x_{i-1})$
Mean	$\frac{1}{N} \sum_i x_i$
Variance	$\frac{1}{N} \sum_i (x_i - \mu)^2$
Skewness	$\frac{1}{N} \sum_i \left( \frac{x_i - \mu}{\sigma} \right)^3$
Kurtosis	$\frac{1}{N} \sum_i \left( \frac{x_i - \mu}{\sigma} \right)^4 - 3$
Spectral Entropy	$-\sum_i P_{xx} \times \log_2(P_{xx})$
Shannon Entropy	$-\sum_i p_i \times \log_2(p_i)$
Renyi Entropy	$\frac{1}{1-q} \log_2 \sum_i p_i^q$
Median Frequency	$\frac{\text{index}(\text{median}(P_{xx})) - 1}{\text{length}(P_{xx} - 1)} \times \frac{F_s}{2}$
Mean Frequency	$\frac{\text{index}(\text{mean}(P_{xx})) - 1}{\text{length}(P_{xx} - 1)} \times \frac{F_s}{2}$
Peak Frequency	$\frac{\text{index}(\text{max}(P_{xx})) - 1}{\text{length}(P_{xx} - 1)} \times \frac{F_s}{2}$

$P_{xx}$  = power spectral density of  $x$ ,  $p_i$  = histogram( $x$ )

any, would be useful in differentiating between the normal and abnormal lobes. Features from multiple domains were extracted to reveal not only temporal characteristics of the time courses but frequency and statistical information as well. In the presence of epileptiform discharges, one might expect higher signal amplitudes and greater oscillations in the perfusion signal due to the increased neuronal activity. These features were chosen because they seem suited to identifying these signal changes and have proven useful in the analysis of other electrophysiological signals such as EEG [9].

After the features were extracted from the CBF image time courses, they were used to classify each voxel in the hippocampus as belonging to either the left or the right hemisphere.

#### D. Genetic Programming

Genetic programming (GP) is a machine learning technique that employs an evolutionary algorithm to generate an optimal program to solve a given problem [10, 11]. Evolutionary algorithms apply genetic operators such as reproduction, mutation, crossover, and selection to find optimal solutions from populations of candidate solutions, also known as individuals or chromosomes. Individuals are assessed through evaluation of a fitness function, which measures the individual's ability to solve the given problem. The result of the algorithm is the individual with the best fitness.

GP is an extension of genetic algorithms (GA), but there are a few key differences. First, unlike GA, which finds a direct solution to a problem, GP outputs a program that can be used to solve the problem. The variably sized GP programs are represented as tree structures; on the other hand, GA chromosomes are fixed-length and are represented as strings or vectors of binary or real values. Because the size of individuals is not fixed in GP, the algorithm is capable of creating both simple and highly complex candidate solutions. Figure 2 shows an example of a GP tree. The gray nodes are functions, and the white nodes are terminals. Functions are arithmetic, mathematical, Boolean, or conditional operators that take arguments, and terminals are user inputs to the GP algorithm.

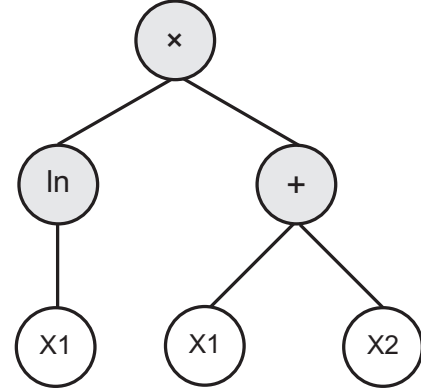


Fig. 2. Tree representation of the GP program  $\ln(X1) \times (X1+X2)$ .

For this study, GP was employed to fuse the thirteen extracted features into one composite feature with increased classification accuracy. The terminals in this case are the thirteen extracted features, and the functions are arithmetic and trigonometric operators applied to the features for fusion. See Table II for a list of the functions used in this experiment. All experiments were performed using the GPLAB genetic programming toolbox for Matlab [12]. To minimize the complexity of the features generated by the GP algorithm, the trees were only allowed to evolve for twenty generations, and the depth of the trees was limited to ten levels. The fitness function used to evaluate each individual,

$$\text{fitness} = \frac{\sqrt{\sigma_1^2 + \sigma_2^2}}{|\mu_1 - \mu_2|} \times \frac{1}{1 - \text{PDF overlap}}, \quad (1)$$

is the inverse of the Fisher discriminant ratio divided by one minus the probability density function (PDF) overlap. The Fisher discriminant ratio (FDR) measures the distance between two classes. Sometimes seemingly good FDR values still produce features with large overlaps in the histograms for the two classes. The fitness function in (1) penalizes individuals with large class overlaps by increasing the fitness score in proportion to the amount overlap. The overlap values range from 0 for no overlap to 1 for total overlap. The individual with the lowest fitness score is ultimately selected as the best.

TABLE II  
GENETIC PROGRAMMING FUNCTIONS

Function	Symbol
Addition	+
Subtraction	-
Multiplication	×
Division	÷
Square	() <sup>2</sup>
Cube	() <sup>3</sup>
Square root	√
Natural logarithm	ln
Absolute value	
Sine	sin
Cosine	cos

### III. RESULTS

Clear evidence of hypoperfusion was found in the epileptogenic hippocampi of all patients except Pt2, who had higher perfusion on the epileptic side. The asymmetry index (AI) was also calculated as a measure of the significance of the difference in the CBF values using the equation

$$AI = 100 \times \frac{(LHC\ CBF) - (RHC\ CBF)}{(LHC\ CBF) + (RHC\ CBF)}, \quad (2)$$

where LHC CBF and RHC CBF are the mean CBF values in the left and right hippocampi, respectively. The higher the asymmetry index, the larger the perfusion difference between the two sides. As found in previous studies there was also asymmetry in perfusion in the hippocampi of the controls but to a lesser extent than most of the patients. These results are summarized in Table III.

TABLE III  
MEAN CBF (IN UNITS OF ML/100G/MIN) IN THE HIPPOCAMPI

Subject	Seizure Side	LHC CBF	RHC CBF	AI
Pt1	Left	78.24	91.60	-7.87
Pt2	Right	59.66	69.60	-7.69
Pt3	Left	49.85	56.62	-6.36
Pt4	Right	37.26	31.77	7.96
Pt5	Left	42.28	46.62	-4.89
Con1	N/A	79.19	86.16	-4.22
Con2	N/A	49.04	48.51	0.54
Con3	N/A	68.40	72.97	-3.23

The feature chosen for initial analysis was the mean CBF of the voxel time courses as mean CBF has already proven to be useful in distinguishing between normal and abnormal mesial temporal lobes when averaged over the entire region. The mean CBF of the voxel-based time course before rescaling to the range [-1,1] was computed for each subject and histograms of the mean values for the two brain hemispheres were calculated. The mean CBF histogram for Pt4 is shown at the top of Figure 3. The overlap between the two classes is extensive.

The thirteen features listed in Table I were extracted from the individual hippocampal voxel-based time courses of each subject to find one or more features capable of separating left and right hippocampal voxels. For this experiment, the

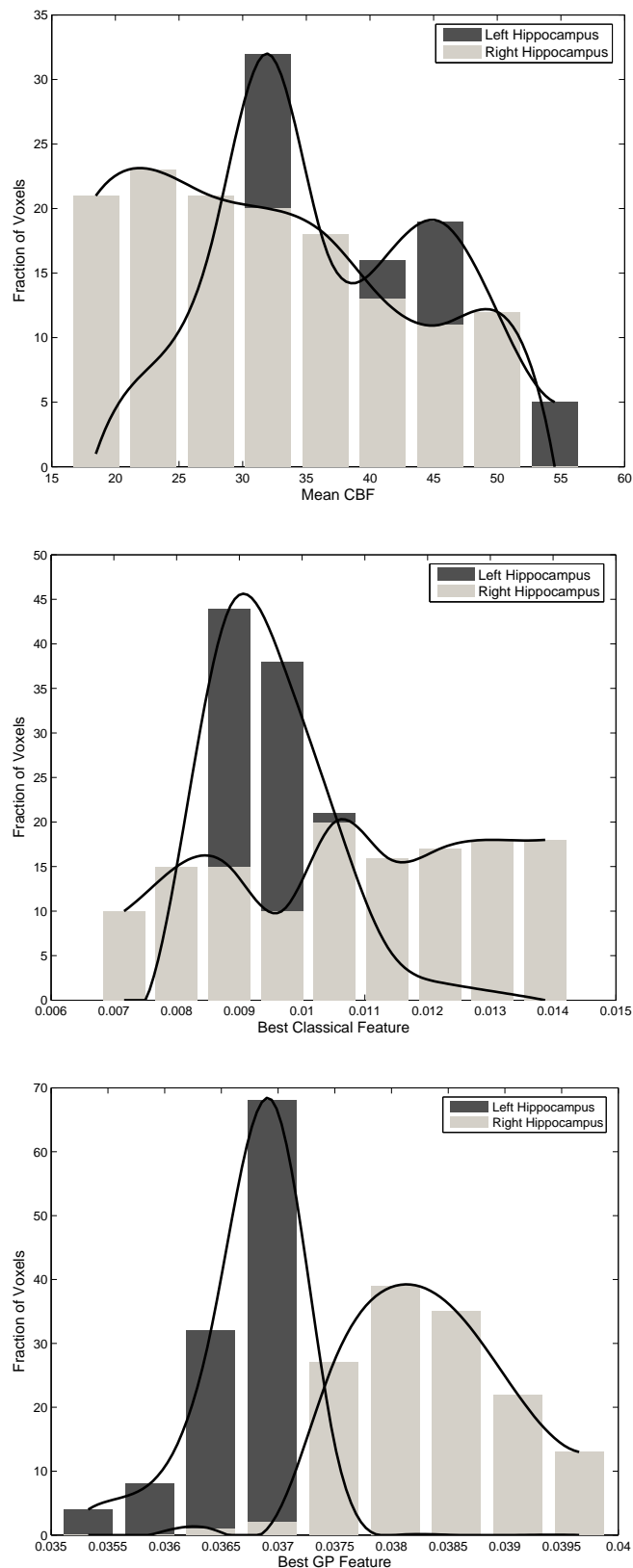


Fig. 3. Feature histograms for Pt4. (Top) The distribution of mean values for the original CBF data. (Middle) The distribution of best classical feature values for the rescaled data. (Bottom) The distribution of GP feature values. The GP feature for this patient is variance ÷ nonlinear energy.

rescaled data was used so that the intrinsic differences in the regional means did not increase the feature separability. The best feature found for each patient and the classification accuracy when thresholding based on these features are listed in Table IV. The histogram of the best classical feature for Pt4 can be seen in the center of Figure 3.

TABLE IV  
BEST CLASSICAL FEATURE FOR CLASS SEPARATION

Subject	Feature	Accuracy	Sensitivity	Specificity
Pt1	Variance	93.26%	94.29%	92.13%
Pt2	Skewness	78.61%	73.20%	85.53%
Pt3	Mean	74.69%	82.20%	67.48%
Pt4	Median Frequency	72.18%	86.61%	58.99%
Pt5	Energy	93.94%	96.00%	91.23%
Con1	Spectral Entropy	80.56%	84.16%	75.95%
Con2	Energy	70.47%	82.43%	58.67%
Con3	Kurtosis	71.63%	57.45%	83.33%

To improve the voxel classification accuracy, the classical features were combined using GP. The set of thirteen features was not reduced using PCA or another feature selection technique because of Cover’s findings in [13], which show that choosing the  $k$  best features ( $k <$  the total number of features  $N$ ) does not always guarantee the highest pattern classification accuracy. Features that perform poorly on an individual basis may provide useful information when combined with other features.

The features created using GP are summarized in Table V. The entries levels and nodes relate to the complexity of the tree. For example, the function illustrated in Figure 2 has three levels and six nodes. Simple features have low numbers of levels and nodes, while the opposite is true for complex features. The number of generations is the number of iterations for which the GP evolved before meeting a stop condition. If a classification accuracy of 95% was reached, the program terminated before reaching the maximum number of generations. Otherwise, the features evolved for twenty generations. The histogram of the best composite feature for Pt4 is shown at the bottom of Figure 3.

TABLE V  
BEST COMPOSITE FEATURE FOR CLASS SEPARATION

Subject	Levels	Nodes	Gen	Acc	Sens	Spec
Pt1	3	4	1	95.88%	95.28%	96.43%
Pt2	8	12	20	84.39%	93.42%	77.32%
Pt3	4	6	20	80.08%	83.74%	76.27%
Pt4	2	3	1	95.49%	92.09%	99.21%
Pt5	3	5	3	96.97%	98.25%	96.00%
Con1	7	10	20	85.00%	79.75%	89.11%
Con2	10	30	20	84.56%	84.00%	85.14%
Con3	10	29	20	85.58%	83.33%	88.30%

Gen = number of generations, Acc = accuracy, Sens = sensitivity, and Spec = specificity

#### IV. DISCUSSION

The measures of mean CBF were concordant with the seizure onset laterality as determined by physicians analyzing

the video EEG, PET, and structural MRI data in four of the five patients. Pt1 and Pt5 exhibited hypoperfusion in the regions where hypometabolism was found during the PET scans. Pt3 had hypometabolism in the hippocampus on the side of seizure onset, and Pt4 also exhibited hypoperfusion in the abnormal lobe despite having a normal PET scan. Pt2 had significantly higher CBF in the epileptogenic right hippocampus than the healthy left. This unexpected result may be related to subclinical electrographic seizures, which typically are not detected by simple observation, during the fMRI acquisition, resulting in an increase in CBF. The perfusion asymmetry in the controls was lower than that in the patients as expected.

While the aggregate CBF values in the hippocampus have the potential to lateralize epilepsy in most patients, the mean CBF of individual voxels varies widely within these regions. As demonstrated by the extensive overlap between the left and right hippocampal voxel CBF values, this feature alone is not enough to classify voxels as normal or abnormal. Labeling based on this feature would be highly inaccurate.

The classical features provided excellent class separation for Pt1 and Pt5, leading to over 93% accuracy in classifying the voxels. As shown in Table IV, the other patients had much lower classification accuracies, so none of the classical features adequately characterized the differences in the temporal dynamics of the CBF signals in the two hippocampi. The same holds true for the controls. Note that the best feature was not the same for each subject. This is most likely due to the presence of large amounts of physiological noise in these data. Physiological noise due to respiration and heartbeat are unique to each patient, so they obscure the underlying CBF signal differently in each patient. Clearly a better feature is needed for classifying individual voxels as belonging to one region or the other. By fusing the individual features into a single feature, knowledge of multiple signal characteristics can be taken into account during the classification process.

Pt1 and Pt5, whose classification accuracies were already high when using a single classical feature, had slightly improved results when the features were fused. After a few iterations of the GP algorithm, features with over 95% classification accuracy were found for both of these patients. The fused features were also quite simple, consisting of few levels and nodes. The classification accuracy for Pt4 had the greatest increase when labeling the voxels based on the GP feature instead of the classical feature. The feature generated for Pt4 was also quite simple and needed only one generation to evolve. The improvement in the class separation can be seen in the decrease in the overlap in the histograms in Figure 3. Pt2 and Pt3 also had increased class separation when using the GP feature, but the generated features took longer to evolve and were complex. The overall accuracy for these patients was much lower than for the other three patients. Improved class separation was also achieved for the controls when using the fused features, but the generated features were very complex and took a long time to evolve, meaning that the GP algorithm was able to distinguish between the left and right hippocampal voxels but with difficulty. The

complexity of the generated features could be a sign that the GP algorithm is the modeling noise rather than the fMRI signals themselves.

## V. CONCLUSION

In this initial series of analyses, features that clearly discriminate epileptogenic brain from normal brain were generated from ASL perfusion fMRI images through feature fusion using genetic programming. The fused features extracted from the left and right hippocampi of the temporal lobe epilepsy patients in this study complemented and improved on the information from the standard perfusion analysis technique of comparing mean blood flow in the two hemispheres. These findings suggest that analysis of the temporal dynamics of voxel time course data in ASL perfusion fMRI images may be useful to distinguish epileptogenic regions from normal brain.

In future work, these GP generated features will be used to find voxels outside of the ROI with similar feature values to those voxels within the epileptogenic zone. Essentially the feature values will be used as a measure of functional connectivity, to see how epileptic activity extends beyond the seizure onset zone. Finding areas outside of the epileptogenic zone with similar temporal characteristics will help to map the larger epileptic network. The enabling technologies include imaging data processing, feature or condition indicator extraction, and classification. Results from this study can be used by physicians to localize areas in the brain that are sources of epileptic activity, and eventually, to control seizures via surgery or electrical stimulation.

## ACKNOWLEDGMENT

The authors thank the Center for Functional Neuroimaging at the University of Pennsylvania for providing the data for this investigation and for advice on how to preprocess the data.

## REFERENCES

- [1] H. Witte, L. D. Iasemidis, and B. Litt, "Special issue on epileptic seizure prediction," *Biomedical Engineering, IEEE Transactions on*, vol. 50, pp. 537-539, 2003.
- [2] J. A. Detre and J. Wang, "Technical aspects and utility of fMRI using BOLD and ASL," *Clinical Neurophysiology*, vol. 113, pp. 621-634, 2002.
- [3] R. L. Wolf, D. C. Alsop, I. Levy-Reis, P. T. Meyer, J. A. Maldjian, J. Gonzalez-Atavales, J. A. French, A. Alavi, and J. A. Detre, "Detection of Mesial Temporal Lobe Hypoperfusion in Patients with Temporal Lobe Epilepsy by Use of Arterial Spin Labeled Perfusion MR Imaging," *AJNR Am J Neuroradiol*, vol. 22, pp. 1334-1341, 2001.
- [4] S. T. Herman, T. S. Walczak, and C. W. Bazil, "Distribution of partial seizures during the sleep-wake cycle: Differences by seizure onset site," *Neurology*, vol. 56, pp. 1453-1459, 2001.
- [5] R. S. J. Frackowiak, K. J. Friston, C. Frith, R. Dolan, C. J. Price, S. Zeki, J. Ashburner, and W. D. Penny, *Human Brain Function*, 2nd ed: Academic Press, 2003.
- [6] J. Wang, Z. Wang, G. K. Aguirre, and J. A. Detre, "To smooth or not to smooth? ROC analysis of perfusion fMRI data," *Magnetic Resonance Imaging*, vol. 23, pp. 75-81, 2005.
- [7] K. J. Friston, J. Ashburner, C. D. Frith, J. B. Poline, J. D. Heather, and R. S. J. Frackowiak, "Spatial registration and normalization of images," *Human Brain Mapping*, vol. 3, pp. 165-189, 1995.
- [8] K. J. Friston, A. P. Holmes, K. J. Worsley, J. P. Poline, C. D. Frith, and R. S. J. Frackowiak, "Statistical parametric maps in functional imaging: A general linear approach," *Human Brain Mapping*, vol. 2, pp. 189-210, 1994.
- [9] M. D'Alessandro, R. Esteller, G. Vachtsevanos, A. Hinson, J. Echauz, and B. Litt, "Epileptic seizure prediction using hybrid feature selection over multiple intracranial EEG electrode contacts: a report of four patients," *IEEE Transactions on Biomedical Engineering*, vol. 50, pp. 603-615, 2003.
- [10] J. R. Koza, *Genetic Programming: On Programming of Computers by Means of Natural Selection*. Cambridge, MA: MIT Press, 1992.
- [11] W. Banzhaf, P. Nordin, R. E. Keller, and F. D. Francone, *Genetic Programming: An Introduction: On the Automatic Evolution of Computer Programs and Its Applications*. San Francisco, CA: Morgan Kaufmann Publishers, Inc., 1998.
- [12] S. Silva and J. Almeida. "GPLAB – A Genetic Programming Toolbox for MATLAB". In Gregersen L (ed), *Proceedings of the Nordic MATLAB Conference (NMC-2003)*, 273-278, 2003.
- [13] T. M. Cover "The Best Two Independent Measurements Are Not the Two Best," *IEEE Transactions on Systems, Man, and Cybernetics*, vol. 4, pp.116-117, 1974.